Nano Research

ISSN 1998-0124 CN 11-5974/O4
https://doi.org/10.1007/s12274-023-6418-7

Research Article

Tertiary orientation structures enhance the piezoelectricity of MXene/PVDF nanocomposite

Yong Ao[1], Tao Yang[1], Guo Tian[1], Shenglong Wang[1], Tianpei Xu[1], Lin Deng[1], Jieling Zhang[1], Lihua Tang[2], Weili Deng[1], Long Jin[1] (✉), and Weiqing Yang[1,3] (✉)

[1] *Key Laboratory of Advanced Technologies of Materials (Ministry of Education), School of Materials Science and Engineering, Southwest Jiaotong University, Chengdu 610031, China*
[2] *Department of Mechanical Engineering, The University of Auckland, Auckland 1010, New Zealand*
[3] *Research Institute of Frontier Science, Southwest Jiaotong University, Chengdu 610031, China*

Received: 10 October 2013 / **Revised:** 3 December 2023 / **Accepted:** 16 December 2023

ABSTRACT

With the increasing demand for flexible piezoelectric sensor components, research on polyvinylidene fluoride (PVDF) based piezoelectric polymers is mounting up. However, the low dipole polarization and disordered polarization direction presented in PVDF hinder further improvement of piezoelectric properties. Here, we constructed an oriented tertiary structure, consisting of molecular chains, crystalline region, and MXene sheets, in MXene/PVDF nanocomposite via a temperature-pressure dual-field regulation method. The highly oriented PVDF molecular chains form approximately 90% of the β phase. In addition, the crystalline region structure with long-range orientation achieves out of plane polarization orientation. The parallel orientation arrangement of MXene effectively enhances the piezoelectric performances of the nanocomposite, and the current output of the device increases by nearly 23 times. This high output device is used to monitor exercise action, exploring the potential applications in wearable electronics.

KEYWORDS

flexible sensor, piezoelectric, MXene/PVDF nanocomposite, orientation structures

1 Introduction

With the development of flexible electronic devices, piezoelectric materials are more critical to meet the demand of exploring advanced sensors. Due to the characteristic of flexibility, biocompatibility, and light weight, polyvinylidene fluoride (PVDF) and its copolymers have a lot of promising applications in human–machine interaction, soft robotics, and health detection [1–7]. However, the piezoelectricity of PVDF needs to be further enhanced for widespread applications. Blending with high piezoelectricity ceramics, as the most traditional method [8, 9], is simple but also inefficient. The as-made composites suffer from mismatched mechanical properties and troublesome interface problems. In order to further improve the piezoelectric properties of PVDF, a deep understanding is needed. Fundamentally, the piezoelectricity of PVDF is based on dipole number and dipole orientation in the crystalline regions [10, 11]. Among the crystalline phases of PVDF, β phase is the most electroactive polar phase due to its all-trans (TTTT) conformation [12]. Accordingly, high β phase content is indispensable to improve piezoelectricity. Chemical modification is an essential method to obtain PVDF with high β phase content and dipole orientation. For example, the introduction of polar units such as trifluoroethylene can effectively enhance the electroactive capacity of molecular chains [13–15]. Nevertheless, the crystallinity of PVDF after chemical modifications may be reduced and accompanied by many defects, which limit the further improvement of PVDF piezoelectricity. Compared with chemical modifications, physical methods are cheaper and more promising for large-scale applications. In recent years, more attentions are attracted on filler-assisted means [8, 16–19]. Specifically, the increase of β phase content can be induced by the electrostatic and interfacial polarization effects of fillers in PVDF [20]. Nowadays, interfacial polarization and interfacial locking effects of two-dimensional (2D) nanofillers have been used to effectively increase the content of β phase and enhance the degree of dipole orientation [17, 21]. However, the random distribution of fillers leads to the disorder of crystalline region and inorganic–organic interfaces, which harm the dipole orientation and spontaneous polarization. Therefore, there is a strong desire to develop a strategy to enhance PVDF's piezoelectricity by both abundant dipole number and oriented distribution of fillers.

In this work, we reported a tertiary oriented structure in MXene ($Ti_3C_2T_x$)/PVDF nanocomposite by the temperature-pressure dual-field regulation for piezoelectricity enhancement. Fundamentally, electrostatic interaction and van der Waals force are induced between MXene and PVDF molecular chains due to the large specific surface area and abundant polar surface functional groups of MXene [22], which are beneficial for increasing the fraction of β phase and crystallinity. The molecular chains in PVDF are oriented to form a large number of β phase and rod-like nanocrystals, under the extreme molding environment provided

Address correspondence to Long Jin, longjin@swjtu.edu.cn; Weiqing Yang, wqyang@swjtu.edu.cn

by the dual fields. In addition, the rod-like nanocrystals in the β phase constitute a laminar oriented crystalline structure, enhancing polarization in the *z*-axis direction. Furthermore, the MXene sheets are arranged in parallel in PVDF after the dual-field regulation, raising the percolation threshold and strengthening the piezoelectric output of the MXene/PVDF based devices. Finally, the fabricated device is demonstrated to monitor different human motions as a wearable sensor.

2 Experimental section

2.1 Preparation of MXene

1.6 g LiF was added to a 9 mol/L HCl solution, and the solution was stirred in an ice bath for 10 min, in order to obtain the etching solution. After that, 1 g Ti_3AlC_2 (MAX) was added to the etching solution, and the mixture was stirred at 40 °C for 24 h to remove the Al in MAX. After etching for 24 h, the mixture was filtered to obtain the reaction product, and washed repeatedly with ultra-pure water until the pH value is greater than 6. MXene ($Ti_3C_2T_x$) powder can be obtained by drying reaction product in vacuum.

2.2 Fabrication of the MXene/PVDF nanocomposite films

Firstly, PVDF powder was dissolved in dimethyl formamide and stirred at 45 °C water bath to prepare 10 wt.% solution. Then, the MXene powder was mixed with PVDF solution and to obtain a homogeneous dispersion by stirring it for 10 h. The MXene/PVDF precursor is separated by deionized water using a non-solvent phase separation method, and then dried in vacuum at 60 °C for 18 h to obtain the dried product. On the basis of the previous, the MXene/PVDF nanocomposite films were obtained via hot-pressing the precursor mentioned above at high temperatures under different pressures, and cooled in the furnace to room temperature.

2.3 Fabrication of the device

The nanocomposite films were cut into a specific shape through an ultraviolet laser marking machine. Two silver electrodes of the nanocomposite films were endowed via magnetron sputtering to form a sandwich structure. Finally, the device was sealed with the polyurethane (PU) tape.

2.4 Characterizations

The morphology of nanocomposite and matrix after etching, MXene, and MXene in matrix was characterized by the scanning electron microscopy (JSM 7800F). X-ray diffraction (Empyrean, PANalytical), X-ray photoelectron spectroscopy (ESCALAB XI+), Raman spectrum (HORIBA Jobin-Yvon XploRA ONE, 532 nm laser), Fourier transform infrared spectroscopy (Nicolet IS50 Spectrometer), small angle X-ray diffraction (Xeuss 2.0), and differential scanning calorimetry (TGA/DSC 3+, Mettler Toledo) were used to characterize crystal content, the phase, and chemical structures of nanocomposite films. Ferroelectric properties of nanocomposite films were characterized by TF Analyzer 2000E equipped with FE-Module at room temperature. Dielectric properties of nanocomposites films were characterized by broad dielectric spectrometer (Concept 80, Novocontrol) at room temperature. The electric output of devices was measured by Keithley 6514, and the motion control system consists of a linear motor (LinMot H01-23×86/160) and a dynamometer (IMADA model ZPS-DPU-50N).

3 Results and discussion

Figures 1(a) and 1(b) illustrate the structure transformation from an isotropic state to an anisotropic state under temperature and pressure fields. Comparing the materials before and after regulation, the conformation of PVDF molecular chains tends to transform from a nonpolar phase (TGTG') to a polar phase (TTTT). The distribution of the crystalline region and MXene in *x*–*y* plane tends to be more parallel oriented. Thus, the tertiary

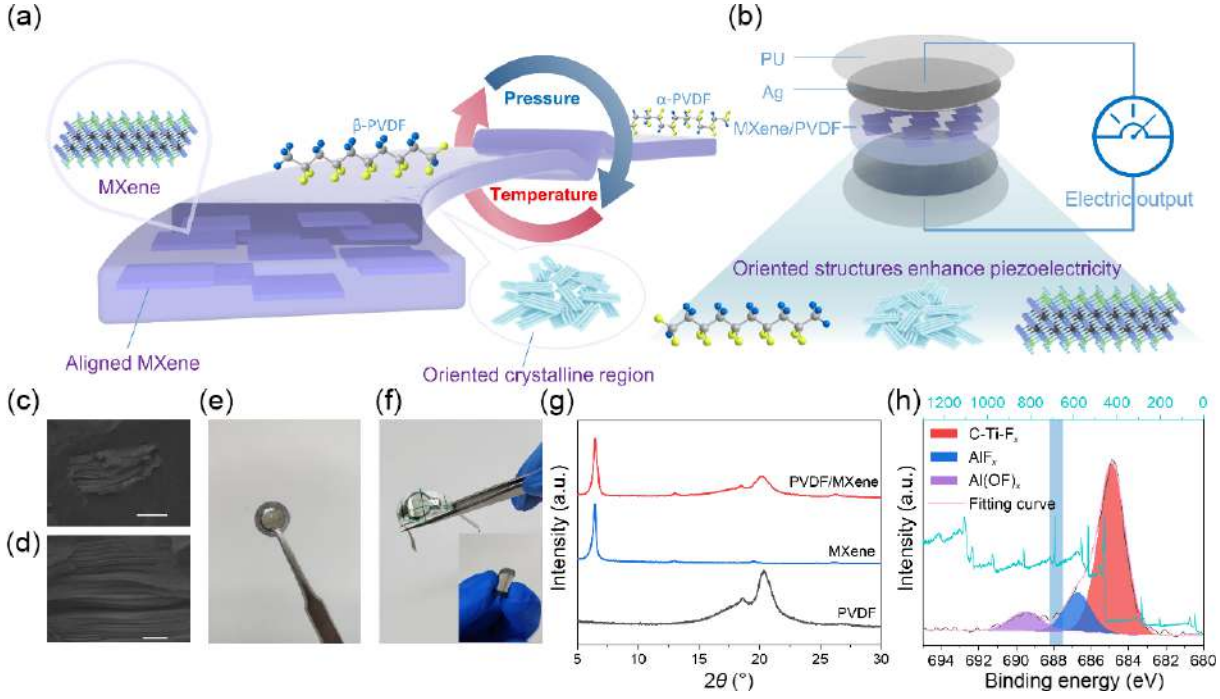

Figure 1 The preparation schematic diagram and characterizations of MXene/PVDF nanocomposite films. (a) Preparation of nanocomposite films with tertiary oriented structure by dual-field regulation. (b) The schematic diagram of MXene/PVDF-based piezoelectric device. (c) SEM image of MXene in the PVDF, presenting the harmonious connection between two materials (scale bar is 3 μm). (d) Partial enlarged view of (c), showing the details of MXene multi-layer structure (scale bar is 500 nm). (e) Photograph of the MXene/PVDF nanocomposite film with Ag electrodes. (f) Photograph of the device with high flexibility. (g) XRD scans of MXene, PVDF, and MXene/PVDF (12 wt.%) nanocomposite films. (h) XPS survey spectra of MXene on a silicon substrate and the binding energy associated with F 1s.

oriented structures of nanocomposite are formed from the microscale to macroscale. More specifically, the tertiary oriented structures are the orientation of molecular chain, crystalline region structure, and orientation distribution of MXene. This kind of oriented structure is helpful to enhance the piezoelectric output of the nanocomposite-based device. Figures 1(c) and 1(d) present MXene in the nanocomposite films, from which the special layered structure and the harmonious combination of MXene with PVDF can be clearly observed. The devices made of nanocomposite films are presented in Figs. 1(e) and 1(f), showing excellent flexibility. MXene can be identified in Figs. S1(a) and S1(b) in the Electronic Supplementary Material (ESM), where the multi-layer structure of MXene is distinct [23]. The X-ray diffraction (XRD) spectra of MXene are presented in Fig. S1(c) in the ESM, where the characteristic peaks from left to right correspond to (002), (004), (006), and (008) crystal planes of MXene respectively [24]. To further study the chemical structures and components of nanocomposite, the nanocomposite films were characterized through XRD, scanning electron microscope (SEM), X-ray photoelectron spectrometer (XPS), and Raman spectroscopy. The results of XRD in Fig. 1(g) illustrate both MXene and PVDF characteristic peaks, where the characteristic peaks of MXene locate at $2\theta = 6.48°$, 12.99°, 19.56°, 26.18° [25, 26], the characteristic peak of β-PVDF locates at $2\theta = 20.26°$, and the peak located at $2\theta = 18.5°$ belongs to γ-PVDF [18, 27]. The results of Raman spectroscopy in Fig. S3 in the ESM reconfirm the successful preparation of MXene/PVDF nanocomposite. The cross-section of nanocomposite film is presented in Fig. S2 in the ESM with energy-dispersive spectrometer (EDS) mapping. The corresponding EDS mapping of C, Ti, and F elements further confirms the homogeneous dispersion of MXene sheets in PVDF. The oxygen content indicates that MXene is well protected by PVDF to prevent oxidation by air. Figure 1(h) shows the XPS spectra of MXene, verifying the fully etching of MAX and the terminal groups of MXene. The peak of F 1s appeals at 685.2 eV, which confirms that there are abundant F-terminated groups on the surface of MXene due to etching solution [28]. As well known, PVDF molecular chains are constructed of the structural unit -CH_2-CF_2-, which vastly facilitates the electrostatic interaction and van der Waals force formation or even hydrogen bonds, such as F–H [21, 29, 30]. These plenty of interactions between MXene and PVDF not only ensure the stability and dispersibility of nanocomposite, but also benefit the orientation structures' formation.

The piezoelectric properties of nanocomposite are related to the total dipole moment. According to Eq. (1) as following, it's helpful to enhance the piezo-output of nanocomposite films by enlarging the molecular polarization, which is also highly efficient for PVDF based piezoelectric nanocomposites [31].

$$P = P_{\text{interfacial}} + P_{\text{molecular}} + P_{\text{ionic}} + P_{\text{electronic}} \quad (1)$$

Therefore, it's necessary to improve the proportion of all-trans conformation (β phase), which is the highest electroactive phase compared to the other phases. In Fig. 2(a), the Fourier transform infrared (FTIR) spectra of nanocomposite films, which have a gradient growth of MXene' concentration, show an evident growth of β phase characteristic peak (around 840 cm^{-1}), while an obvious decrease of α phase characteristic peak (around 766 cm^{-1}) [8, 12, 32]. As shown in Fig. 2(b), the crystallinity of PVDF improves with the increase of MXene content. In the nanocomposite, MXene not only acts as a nucleating agent to improve the crystallinity, but also provides van der Waals force and electrostatic attraction with PVDF, as the main factors of conformation change (Fig. 2(c)). Thus, it makes for the net dipole moment perpendicular to the plane of MXene. However, the promotion of MXene to the conformation change of molecular chains is limited, considering the nanometer-level interaction at the interface. In order to improve the content of β phase and oriented polarization, the nanocomposite films are prepared in both temperature and pressure fields. In regard to the melting temperature of β crystallites and the addition of MXene, the temperature varies from 165 to 195 °C. In Fig. 2(d), three characteristic peaks are marked out. The adsorption peak at 766 cm^{-1} is identified to α phase and the peak appeared at 1279 cm^{-1} is the characteristic for β phase, while the adsorption peak at 840 cm^{-1} is considered as common to β phase. As the preparation temperature raising up, the phase structures change accordingly. The 175 °C is a dividing point as illustrated in Figs. 2(d) and 2(g), and the β phase dominates below 175 °C. When the temperature rises above 175 °C, the polymer molecular chains tend to keep thermodynamically stable [33], resulting in a stronger intensity of characteristic peak at 766 cm^{-1} and a weaker characteristic peak at 840 cm^{-1}. There is no significant difference in β phase content when temperature is below 175 °C. However, a higher temperature is beneficial for decreasing defects. On the previous basis, the nanocomposite films were prepared under different pressures at a temperature gradient around 175 °C, since the melting temperature of the β crystallites under atmospheric pressure is around 175 °C. The FTIR spectra of nanocomposite films are presented in Fig. S4 in the ESM and Fig. 2(f). In normal or low pressure conditions, the β phase in the nanocomposite is greatly affected by the raising temperature [34, 35], while a higher preparation pressure is profit to prevent the electroactive phase from switching to non-α phase. Fundamentally, the high-pressure condition reduces the free volume and improves the packing density of chains, which prevents the relaxation of molecular chains at a high temperature [36]. After the dual-field regulation, β phase has a dominant proportion in the nanocomposite film, which reflects the effective construction of molecular chain orientation in the nanocomposite. In Figs. 2(h) and 2(i), the ferroelectric property of the nanocomposite has been also characterized. The preparation methods of electrode and polarization are presented in Fig. S5 in the ESM. From the polarization–electric field (P–E) loops of the nanocomposite, it can be analyzed that the nanocomposite has the characteristics of ferroelectrics. Meanwhile, it can be observed that the sample cannot reach the maximum polarization unless further enhancing the electric field. In addition, the coercive electric fields under different electric fields are relatively low, indicating the reduction of energy barrier for polarization reversal. Accordingly, it is considered that the average size of ferroelectric domains decreases after the dual fields' regulation.

After regulating by dual fields, it is reasonable to speculate that some special structures are formed in the crystalline region. Therefore, the nanocomposite films were detected by the small angle X-ray diffraction (SAXS). In Figs. 3(a) and 3(b), the two-dimensional (2D-SAXS) and one-dimensional (1D-SAXS) profiles present 2 weak diffused spots in the direction with an angle of 45° to the equator line and a scattering peak at 0.46 nm^{-1}, revealing that the crystalline region has a long period of orientation [37]. In order to display the orientation characteristic of the crystalline region more visibly, the nanocomposite film has been etched to expose its rod-like nanocrystals (Fig. 3(c)). According to the previous study, the striations of β phase extended-chain crystallites are parallel to the molecular chains [18, 32, 33, 38], which is beneficial to the piezoelectric output in z-axis of films. Figure S6(a) in the ESM shows the cross section of etched nanocomposite film, which clearly shows the layered structure and how the rod-like nanocrystals constitute it. Figure S6(b) in the ESM provides the top view of the layered structure. On the basis, it is clear that the

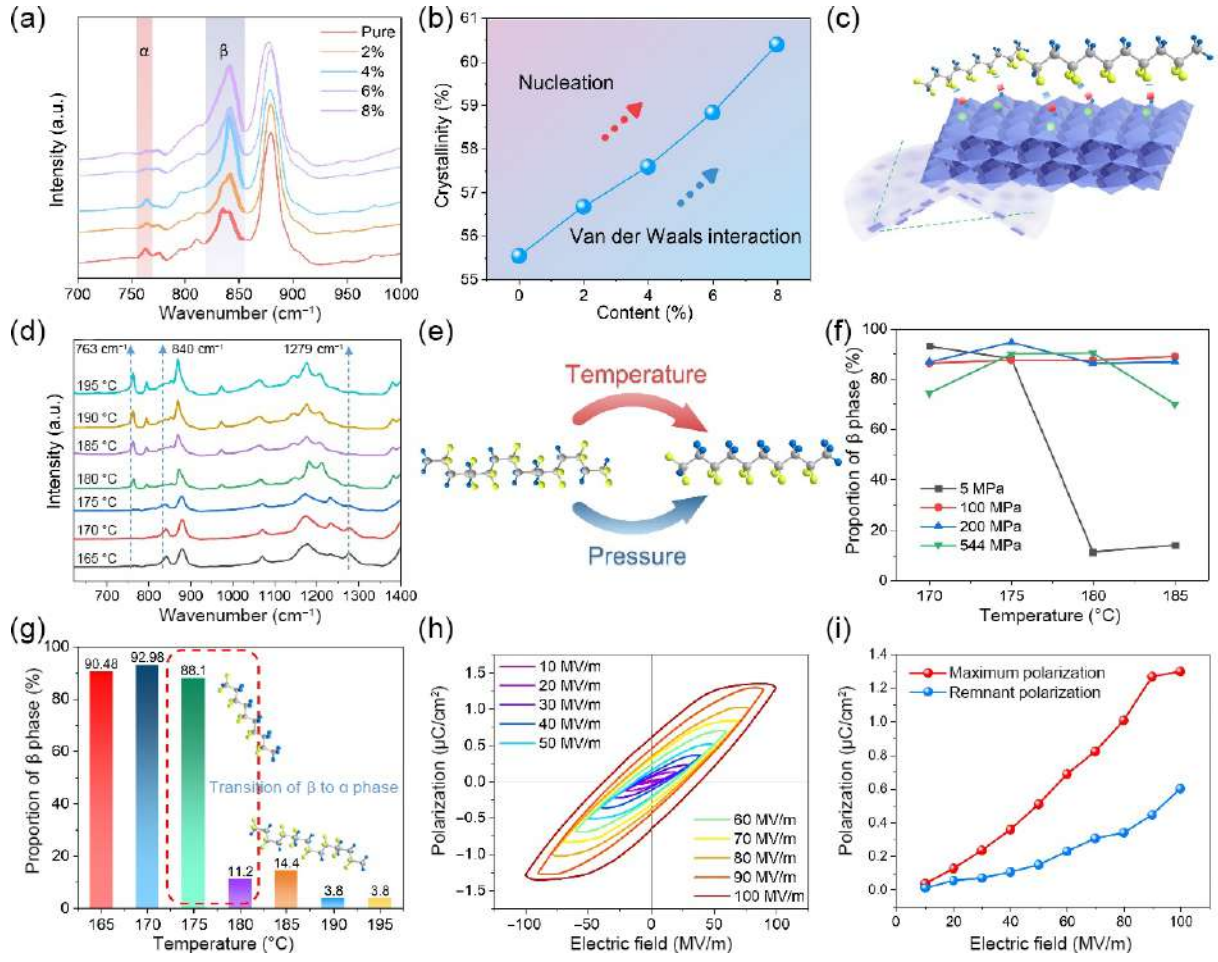

Figure 2 Polymer chain orientation after dual-field regulation. (a) FTIR spectra of MXene/PVDF nanocomposite films with MXene contents from 0% to 8%. (b) The crystallinity of nanocomposite films with different MXene contents (the calculation method is presented Note S1 in the ESM). (c) Schematic diagram of van der Waals force between MXene and polymer chains. (d) FTIR spectra of nanocomposite films prepared at a temperature gradient from 165 to 195 °C. (e) Schematic diagram of polymer chains conformation transition regulated by dual fields. (f) The proportion of β phase in nanocomposite films prepared at a temperature gradient from 165 to 195 °C (the calculation method is presented Note S1 in the ESM). (g) The proportion of β phase in nanocomposite films prepared under dual fields. (h) Hysteresis loops of nanocomposite film under different electric fields at room temperature. (i) The maximum and remnant polarization of nanocomposite film under different electric fields at room temperature.

molecular chains are oriented, resulting in the nanocrystals prior to growth in its *c*-axis. The nanocrystals assemble the layered structure under the high pressure filed, which is oriented and parallel to *x*–*y* plane [38]. According to the ferroelectrics results in Fig. 2(h), there should be a certain number of ferroelectric domains in the nanocrystallites and the net dipole moment has a trend to *z*-axis under the electric field, since the molecular chains and the crystalline region are both oriented (Fig. 3(d)). Besides, some oriented amorphous chains should be also affected by the electric field and contribute to the enhancement of net dipole moment on the *z*-axis [13, 39]. The enhancement of net dipole moment is beneficial to the improvement of polarization on the *z*-axis and piezoelectricity of nanocomposite films.

The MXene tends to have an alignment distribution in nanocomposite films, owing to the regulation of dual fields (the cross-section of nanocomposite film is presented in Fig. 3(e). The net dipole moment around the surface of MXene should prefer the *z*-axis orientation, combining the speculation above. Besides, this kind of parallel distribution can make the percolation threshold move towards a higher concentration, allowing the addition of MXene with a higher concentration [40]. In the Fig. 3(f), it illustrates the permittivity of the nanocomposite films increases with the increase in MXene content, and the permittivity–frequency curves of nanocomposite films are shown in Fig. S7 in the ESM. What's more, Fig. 3(g) shows the parallel distribution of MXene could prevent the bridging of MXene sheets and generation of leakage current at a specific concentration. Therefore, the relation between piezoelectric output and MXene content of nanocomposite should be detected. The results of the current output of devices, which are detected under same pressure and prepared by the nanocomposite with different MXene contents, are presented in Fig. 3(h). From Fig. 3(h), it can easily observe that the percolation threshold is around 12% of MXene content, and the output of devices decreases once the MXene content over the percolation threshold, which is attributed to the generation of plenty of connection when the amount of MXene is excessive (Fig. S8 in the ESM). In order to have an intuitive understanding of the device output, we compared it with previous work (Table S1 in the ESM). Therefore, this concentration was used for the devices in the subsequent parts of this paper in order to have a high output.

It is believed that the mechanical performances of materials are crucial parameters in further applications. The relevant measurement results of the nanocomposite are presented in Fig. S9 in the ESM. It is observed that the Young's modulus and yield strength of the nanocomposites reach their peak values when the MXene content is 12% (Young's modulus: 693.43 MPa; yield strength: 38.29 MPa) and decrease when the content exceeds 12%. For further applications, the electrical performances of materials have been detected through a linear motor and Keithley 6514 (the test condition and equipment are presented in Fig. S10 in the ESM). Firstly, the dependence of piezo-output on pressure had

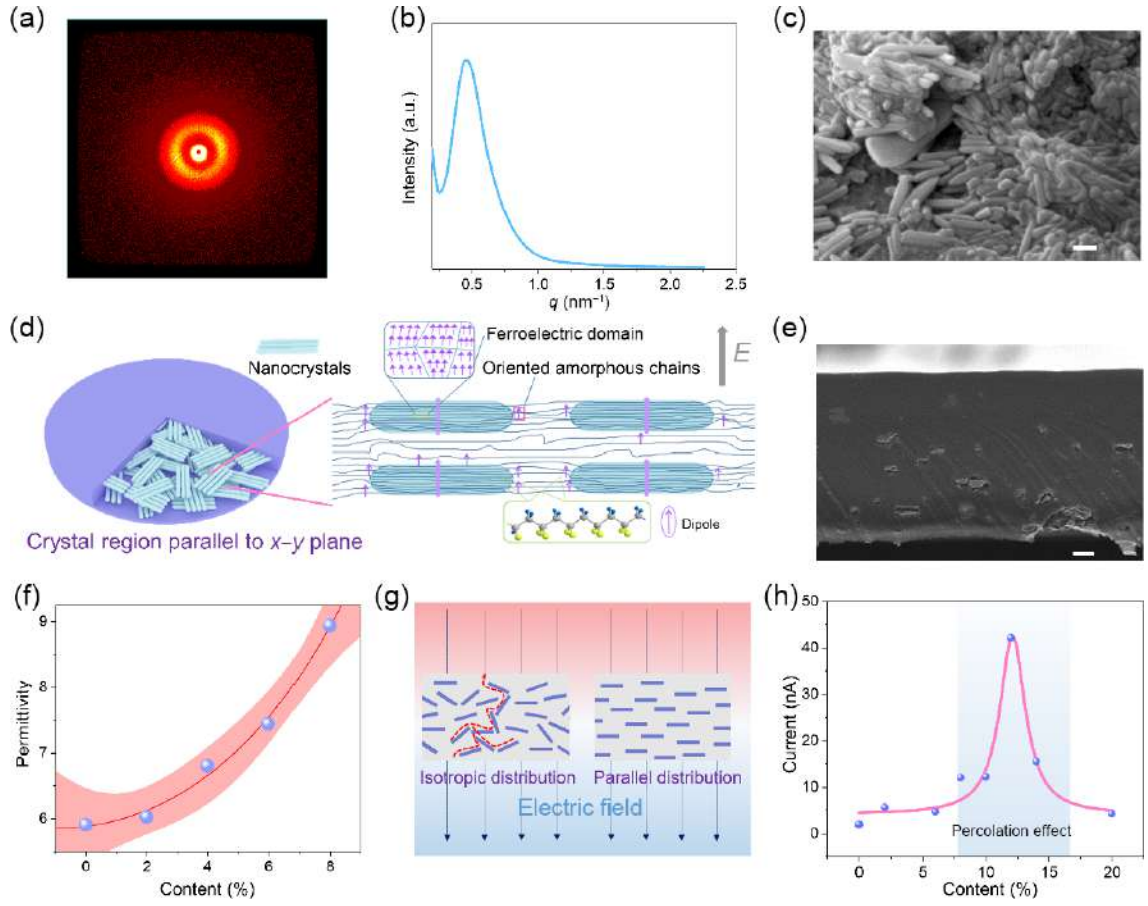

Figure 3 The orientation of crystalline region and MXene distribution after dual-field regulation. (a) 2D-SAXS patterns and (b) 1D-SAXS profiles of MXene/PVDF nanocomposite films. (c) SEM image of crystalline region exposed after etching the amorphous region (scale bar is 200 nm). (d) Schematic diagram of *z*-axis polarization enhanced by oriented crystalline region in nanocomposite films. (e) Cross-section of MXene/PVDF nanocomposite film (scale bar is 10 μm). (f) Permittivity of nanocomposite films with a raising MXene content under 1 Hz. (g) Schematic diagram of parallel arranging MXene to improve the percolation threshold of nanocomposite films. (h) Piezoelectric current output of devices prepared by nanocomposite films with a raising MXene content.

been studied. The current output of device has a linear relationship with the pressure in both low-pressure (< 12 kPa) and high-pressure (above 12 kPa) areas, as shown in Fig. 4(a). The sensitivities of device in both low-pressure and high-pressure areas are calculated, where the value in low pressure is nearly ten times to that in high pressure. The plunge of sensitivity could be attributed to the theoretical threshold for effective deformation, which is inherent to piezo-materials [41]. Then, devices were used to charge a 0.1 μF capacitor at three different working frequency under 28.74 kPa for exploring the potential application in the energy harvest field. The device's charging curve is shown in Fig. 4(b), where the charging rate is positively correlated with the operating frequency, which is consistent with the reality. However, the voltage curve is not a smooth growth, but a stepwise climb, which is caused by the interval time between two compression processes. For example, there are two pulse peaks every second in the charging curve of 2 Hz (Figs. S11(a) and S11(b) in the ESM), and each charging process is attributed to each single piezoelectric output in the long-term output [42]. The impedance of device is also tested (Fig. 4(c)) for the sake of matching the terminal with appropriate resistance and maximizing the output power of device [43, 44]. It is clear that when the load resistance approaches around 40 MΩ, the output power of device comes to a peak. In consideration of above results, the devices have potential applications in the field of energy collection and flexible wearable electronics (Fig. S11(c) in the ESM). It is also available to apply the device in the field of sensing. In Fig. 4(d), it presents a fast response and recovery time of the devices under the pressure of 28.74 kPa. Here, the devices were applied in detecting four kinds of exercise actions (Fig. 4(f) illustrates the testing process), which are namely walking, running, sit-up, and push-up (Figs. 4(e) and 4(g)), for exploring the potential application of exercise assisted intelligent wearable monitoring (Movies ESM1, ESM2, and ESM3). To test the durability of device for long-term using, the device has been applied more than 10,000 cycles and there was no significant performance degeneration (Fig. 4(h)).

4 Conclusions

In summary, this work fabricated a kind of MXene/PVDF nanocomposite with tertiary oriented structure from micro to macro through temperature and pressure fields' regulation. It provides a new method for enhancing the piezoelectricity of materials. The dual-field regulation has made the nanocomposite switching from isotropic to anisotropic in condensed matter structure. Owing to the dual-field regulation and electrostatic attraction, the molecular chains are oriented and the β phase has a domination in the nanocomposite, and the rod-like nanocrystal turns to be the major crystalline form. Under the high-pressure forming condition, a long-range orientation structure appears in the crystalline region of the polymer, where the nanocrystallites form a kind of lamellar crystal structure. This oriented structure increases the number of dipole and enhances the net dipole moment and the polarization of nanocomposite films at the *z*-axis, resulting in the enhancement of piezoelectricity. Besides, the MXene in the nanocomposite has an alignment distribution, which benefits the promotion of devices' piezoelectricity output. Then, the electrical performances of devices are measured for

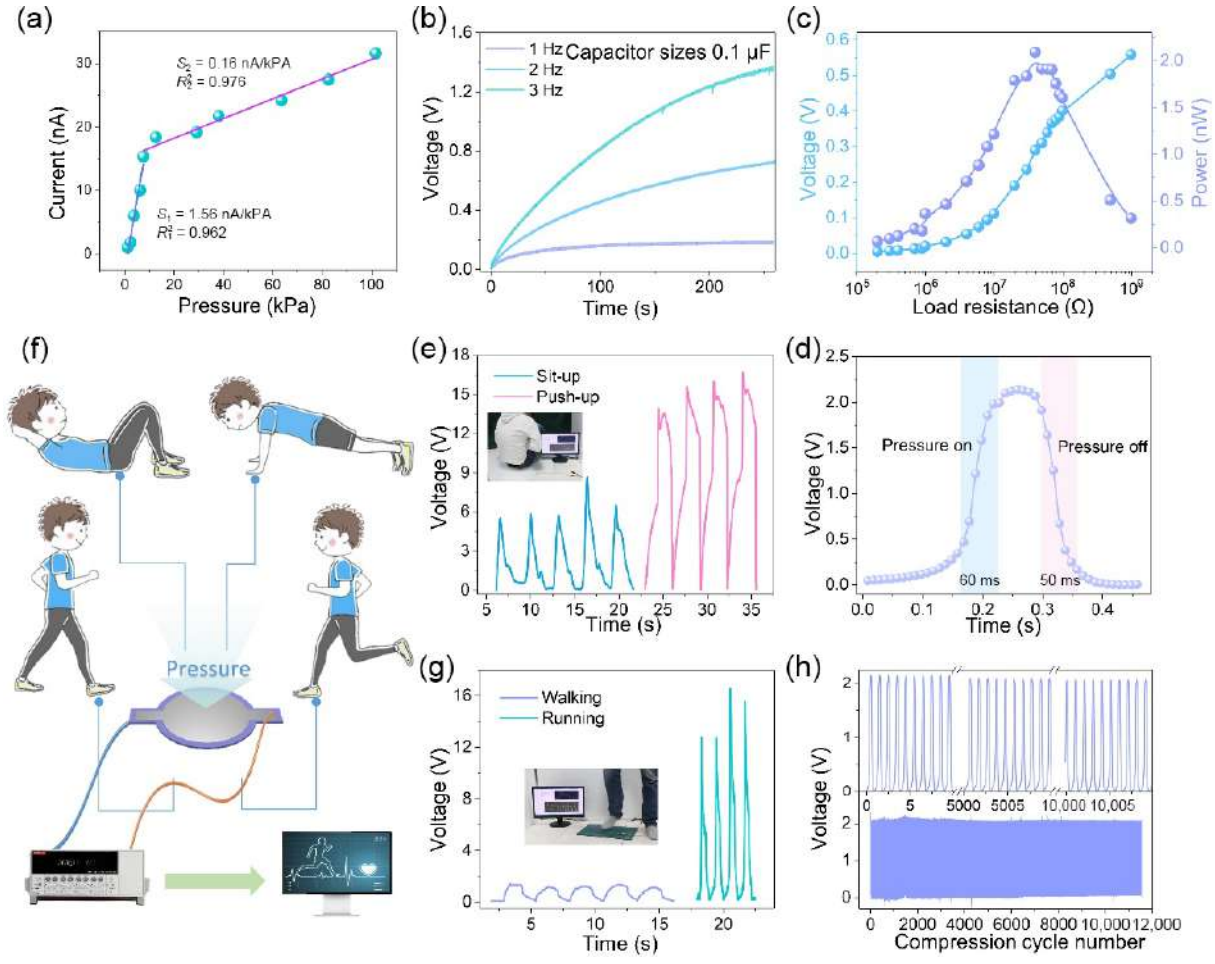

Figure 4 Electric properties and applications of devices. (a) Output current of device under various force and the fit lines of the relationship between current and pressure. (b) Charging curves of devices under different frequencies. (c) Output power and output voltage of the device at resistances vary under 12.74 kPa. (d) Response time of the device under 28.74 kPa. (e) Voltage signals of sit-up and push-up actions detected by devices. The inset photograph shows the testing scene. (f) Applications of the wearable device for energy harvesting and sensing. (g) Voltage signals of walking and running actions detected by the device under the foot. The inset photograph shows the testing scene. (h) Durability test of wearable device by applying more than 10,000 cycles under 28.74 kPa and the expanded initial, middle, and end regions of the output voltage stability data in showing 10 cycles in each panel.

exploring potential applications. Finally, the devices are used to detect four kinds of exercise action, and the results indicate a possible application of exercise assisted intelligent wearable monitoring.

Acknowledgements

This work was financially supported by the National Natural Science Foundation of China (No. 52303328), the Postdoctoral Innovation Talents Support Program (No. BX20220257), the Multiple Clean Energy Harvesting System (No. YYF20223026), the Sichuan Science and Technology Program (No. 2023NSFSC0313), and a Catalyst Seeding General Grant administered by the Royal Society of New Zealand (Contract 20-UOA-035-CSG). We are grateful for the help from the Analysis and Testing Center of Southwest Jiaotong University.

Electronic Supplementary Material: Supplementary material (characterizations of the composite film, testing method, current response, and applications of the film) is available in the online version of the article at https://doi.org/10.1007/s12274-023-6418-7.

References

[1] Qian, X. S.; Chen, X.; Zhu, L.; Zhang, Q. M. Fluoropolymer ferroelectrics: Multifunctional platform for polar-structured energy conversion. *Science* **2023**, *380*, eadg0902.

[2] Chen, G. R.; Li, Y. Z.; Bick, M.; Chen, J. Smart textiles for electricity generation. *Chem. Rev.* **2020**, *120*, 3668–3720.

[3] Deng, W. L.; Zhou, Y. H.; Libanori, A.; Chen, G. R.; Yang, W. Q.; Chen, J. Piezoelectric nanogenerators for personalized healthcare. *Chem. Soc. Rev.* **2022**, *51*, 3380–3435.

[4] Ribeiro, C.; Costa, C. M.; Correia, D. M.; Nunes-Pereira, J.; Oliveira, J.; Martins, P.; Gonçalves, R.; Cardoso, V. F.; Lanceros-Méndez, S. Electroactive poly(vinylidene fluoride)-based structures for advanced applications. *Nat. Protoc.* **2018**, *13*, 681–704.

[5] Ning, C. Y.; Zhou, Z. N.; Tan, G. X.; Zhu, Y.; Mao, C. B. Electroactive polymers for tissue regeneration: Developments and perspectives. *Progr. Polym. Sci.* **2018**, *81*, 144–162.

[6] Cui, N. Y.; Gu, L.; Liu, J. M.; Bai, S.; Qiu, J. W.; Fu, J. C.; Kou, X. L.; Liu, H.; Qin, Y.; Wang, Z. L. High performance sound driven triboelectric nanogenerator for harvesting noise energy. *Nano Energy* **2015**, *15*, 321–328.

[7] Yu, J. B.; Hou, X. J.; He, J.; Cui, M.; Wang, C.; Geng, W. P.; Mu, J. L.; Han, B.; Chou, X. J. Ultra-flexible and high-sensitive triboelectric nanogenerator as electronic skin for self-powered human physiological signal monitoring. *Nano Energy* **2020**, *69*, 104437.

[8] Su, Y. J.; Li, W. X.; Cheng, X. X.; Zhou, Y. H.; Yang, S.; Zhang, X.; Chen, C. X.; Yang, T. N.; Pan, H.; Xie, G. Z. et al. High-performance piezoelectric composites via β phase programming. *Nat. Commun.* **2022**, *13*, 4867.

[9] Peng, S. M.; Yang, X.; Yang, Y.; Wang, S. J.; Zhou, Y.; Hu, J.; Li, Q.; He, J. L. Direct detection of local electric polarization in the interfacial region in ferroelectric polymer nanocomposites. *Adv. Mater.* **2019**, *31*, 1807722.

[10] Huang, Y. F.; Rui, G. C.; Li, Q.; Allahyarov, E.; Li, R. P.; Fukuto, M.; Zhong, G. J.; Xu, J. Z.; Li, Z. M.; Taylor, P. L. et al. Enhanced piezoelectricity from highly polarizable oriented amorphous fractions in biaxially oriented poly(vinylidene fluoride) with pure betaβ crystals. *Nat. Commun.* **2021**, *12*, 675.

[11] Hafner, J.; Benaglia, S.; Richheimer, F.; Teuschel, M.; Maier, F. J.; Werner, A.; Wood, S.; Platz, D.; Schneider, M.; Hradil, K. et al. Multi-scale characterisation of a ferroelectric polymer reveals the emergence of a morphological phase transition driven by temperature. *Nat. Commun.* **2021**, *12*, 152.

[12] Martins, P.; Lopes, A. C.; Lanceros-Mendez, S. Electroactive phases of poly(vinylidene fluoride): Determination, processing and applications. *Progr. Polym. Sci.* **2014**, *39*, 683–706.

[13] Qian, X. S.; Han, D. L.; Zheng, L. R.; Chen, J.; Tyagi, M.; Li, Q.; Du, F. H.; Zheng, S. Y.; Huang, X. Y.; Zhang, S. H. et al. High-entropy polymer produces a giant electrocaloric effect at low fields. *Nature* **2021**, *600*, 664–669.

[14] Liu, Y.; Aziguli, H.; Zhang, B.; Xu, W. H.; Lu, W. C.; Bernholc, J.; Wang, Q. Ferroelectric polymers exhibiting behaviour reminiscent of a morphotropic phase boundary. *Nature* **2018**, *562*, 96–100.

[15] Liu, Y.; Zhang, B.; Xu, W. H.; Haibibu, A.; Han, Z. B.; Lu, W. C.; Bernholc, J.; Wang, Q. Chirality-induced relaxor properties in ferroelectric polymers. *Nat. Mater.* **2020**, *19*, 1169–1174.

[16] Shen, X.; Zheng, Q. B.; Kim, J. K. Rational design of two-dimensional nanofillers for polymer nanocomposites toward multifunctional applications. *Progr. Mater. Sci.* **2021**, *115*, 100708.

[17] Shepelin, N. A.; Sherrell, P. C.; Skountzos, E. N.; Goudeli, E.; Zhang, J. Z.; Lussini, V. C.; Imtiaz, B.; Usman, K. A. S.; Dicinoski, G. W.; Shapter, J. G. et al. Interfacial piezoelectric polarization locking in printable $Ti_3C_2T_x$ MXene-fluoropolymer composites. *Nat. Commun.* **2021**, *12*, 3171.

[18] Yuan, X. T.; Yan, A.; Lai, Z. W.; Liu, Z. H.; Yu, Z. H.; Li, Z. M.; Cao, Y.; Dong, S. X. A poling-free PVDF nanocomposite via mechanically directional stress field for self-powered pressure sensor application. *Nano Energy* **2022**, *98*, 107340.

[19] Zhou, J.; Hou, D. J.; Cheng, S.; Zhang, J. S.; Chen, W.; Zhou, L.; Zhang, P. C. Recent advances in dispersion and alignment of fillers in PVDF-based composites for high-performance dielectric energy storage. *Mater. Today Energy* **2022**, *31*, 101208.

[20] Tian, G.; Deng, W. L.; Yang, T.; Xiong, D.; Zhang, H. R.; Lan, B. L.; Deng, L.; Zhang, B. B.; Jin, L.; Huang, H. C. et al. Insight into interfacial polarization for enhancing piezoelectricity in ferroelectric nanocomposites. *Small* **2023**, *19*, 2207947.

[21] Tian, G.; Deng, W. L.; Xiong, D.; Yang, T.; Zhang, B. B.; Ren, X. R.; Lan, B. L.; Zhong, S.; Jin, L.; Zhang, H. R. et al. Dielectric micro-capacitance for enhancing piezoelectricity via aligning MXene sheets in composites. *Cell Rep. Phys. Sci.* **2022**, *3*, 100814.

[22] Li, X. L.; Huang, Z. D.; Shuck, C. E.; Liang, G. J.; Gogotsi, Y.; Zhi, C. Y. MXene chemistry, electrochemistry and energy storage applications. *Nat. Rev. Chem.* **2022**, *6*, 389–404.

[23] Xiong, D.; Deng, W. L.; Tian, G.; Zhang, B. B.; Zhong, S.; Xie, Y. T.; Yang, T.; Zhao, H. B.; Yang, W. Q. Controllable *in-situ*-oxidization of 3D-networked $Ti_3C_2T_X$-TiO_2 photodetectors for large-area flexible optical imaging. *Nano Energy* **2022**, *93*, 106889.

[24] Shekhirev, M.; Shuck, C. E.; Sarycheva, A.; Gogotsi, Y. Characterization of MXenes at every step, from their precursors to single flakes and assembled films. *Progr. Mater. Sci.* **2021**, *120*, 100757.

[25] Zhang, J. Z.; Kong, N.; Uzun, S.; Levitt, A.; Seyedin, S.; Lynch, P. A.; Qin, S.; Han, M. K.; Yang, W. R.; Liu, J. Q. et al. Scalable manufacturing of free-standing, strong $Ti_3C_2T_x$ MXene films with outstanding conductivity. *Adv. Mater.* **2020**, *32*, 2001093.

[26] Wang, S. L.; Deng, W. L.; Yang, T.; Ao, Y.; Zhang, H. R.; Tian, G.; Deng, L.; Huang, H. C.; Huang, J. F.; Lan, B. L. et al. Bioinspired MXene - based piezoresistive sensor with two - stage enhancement for motion capture. *Adv. Funct. Mater.* **2023**, *33*, 2214503.

[27] Lan, B. L.; Xiao, X.; Carlo, A. D.; Deng, W. L.; Yang, T.; Jin, L.; Tian, G.; Ao, Y.; Yang, W. Q.; Chen, J. Topological nanofibers enhanced piezoelectric membranes for soft bioelectronics. *Adv. Funct. Mater.* **2022**, *32*, 2207393.

[28] Halim, J.; Cook, K. M.; Naguib, M.; Eklund, P.; Gogotsi, Y.; Rosen, J.; Barsoum, M. W. X-ray photoelectron spectroscopy of select multi-layered transition metal carbides (MXenes). *Appl. Surf. Sci.* **2016**, *362*, 406–417.

[29] Su, Y. J.; Chen, C. X.; Pan, H.; Yang, Y.; Chen, G. R.; Zhao, X.; Li, W. X.; Gong, Q. C.; Xie, G. Z.; Zhou, Y. H. et al. Muscle fibers inspired high-performance piezoelectric textiles for wearable physiological monitoring. *Adv. Funct. Mater.* **2021**, *31*, 2010962.

[30] Liu, Y. L.; Tong, W. S.; Wang, L. C.; Zhang, P. P.; Zhang, J. H.; Wang, X. M.; Zhang, S.; Liu, Y.; Liu, S. L.; Wang, S. Q. et al. Phase separation of a PVDF–HFP film on an ice substrate to achieve self-polarisation alignment. *Nano Energy* **2023**, *106*, 108082.

[31] Liu, Z. K.; Li, X. Y.; Zhang, Q. M. Maximizing the number of coexisting phases near invariant critical points for giant electrocaloric and electromechanical responses in ferroelectrics. *Appl. Phys. Lett.* **2012**, *101*, 082904.

[32] Tian, G.; Deng, W. L.; Gao, Y. Y.; Xiong, D.; Yan, C.; He, X. B.; Yang, T.; Jin, L.; Chu, X.; Zhang, H. T. et al. Rich lamellar crystal baklava-structured PZT/PVDF piezoelectric sensor toward individual table tennis training. *Nano Energy* **2019**, *59*, 574–581.

[33] Li, Y.; Tang, S. D.; Pan, M. W.; Zhu, L.; Zhong, G. J.; Li, Z. M. Polymorphic extended-chain and folded-chain crystals in poly(vinylidene fluoride) achieved by combination of high pressure and Ion-dipole interaction. *Macromolecules* **2015**, *48*, 8565–8573.

[34] He, S.; Guo, M. F.; Wang, Y.; Liang, Y. H.; Shen, Y. An optical/ferroelectric multiplexing multidimensional nonvolatile memory from ferroelectric polymer. *Adv. Mater.* **2022**, *34*, 2202181.

[35] Liu, Y.; Zhou, Y.; Qin, H. C.; Yang, T. N.; Chen, X.; Li, L.; Han, Z. B.; Wang, K.; Zhang, B.; Lu, W. C. et al. Electro-thermal actuation in percolative ferroelectric polymer nanocomposites. *Nat. Mater.* **2023**, *22*, 873–879.

[36] Meng, N.; Ren, X. T.; Santagiuliana, G.; Ventura, L.; Zhang, H.; Wu, J. Y.; Yan, H. X.; Reece, M. J.; Bilotti, E. Ultrahigh β-phase content poly(vinylidene fluoride) with relaxor-like ferroelectricity for high energy density capacitors. *Nat. Commun.* **2019**, *10*, 4535.

[37] Ren, J. Y.; Ouyang, Q. F.; Ma, G. Q.; Li, Y.; Lei, J.; Huang, H. D.; Jia, L. C.; Lin, H.; Zhong, G. J.; Li, Z. M. Enhanced dielectric and ferroelectric properties of poly(vinylidene fluoride) through annealing oriented crystallites under high pressure. *Macromolecules* **2022**, *55*, 2014–2027.

[38] Zhang, D. P.; Tian, P. F.; Chen, X.; Lu, J.; Huang, R. Pressure-crystallized piezoelectric structures in binary fullerene C70/poly(vinylidene fluoride) based composites. *J. Appl. Polymer Sci.* **2013**, *130*, 1823–1833.

[39] Jin, L.; Ma, S. Y.; Deng, W. L.; Yan, C.; Yang, T.; Chu, X.; Tian, G.; Xiong, D.; Lu, J.; Yang, W. Q. Polarization-free high-crystallization β-PVDF piezoelectric nanogenerator toward self-powered 3D acceleration sensor. *Nano Energy* **2018**, *50*, 632–638.

[40] Huang, X. Y.; Sun, B.; Zhu, Y. K.; Li, S. T.; Jiang, P. K. High-*k* polymer nanocomposites with 1D filler for dielectric and energy storage applications. *Progr. Mater. Sci.* **2019**, *100*, 187–225.

[41] Zhang, J. L.; Yang, T.; Tian, G.; Lan, B. L.; Deng, W. L.; Tang, L. H.; Ao, Y.; Sun, Y.; Zeng, W. H.; Ren, X. R. et al. Spatially confined MXene/PVDF nanofiber piezoelectric electronics. *Adv. Fiber Mater.*, in press, DOI: 10.1007/s42765-023-00337-w.

[42] Yang, T.; Pan, H.; Tian, G.; Zhang, B. B.; Xiong, D.; Gao, Y. Y.; Yan, C.; Chu, X.; Chen, N. J.; Zhong, S. et al. Hierarchically structured PVDF/ZnO core–shell nanofibers for self-powered physiological monitoring electronics. *Nano Energy* **2020**, *72*, 104706.

[43] Yun, J.; Park, J.; Ryoo, M.; Kitchamsetti, N.; Goh, T. S.; Kim, D. Piezo-triboelectric hybridized nanogenerator embedding MXene based bifunctional conductive filler in polymer matrix for boosting electrical power. *Nano Energy* **2023**, *105*, 108018.

[44] Yu, J. B.; Xian, S.; Zhang, Z. P.; Hou, X. J.; He, J.; Mu, J. L.; Geng, W. P.; Qiao, X. J.; Zhang, L.; Chou, X. J. Synergistic piezoelectricity enhanced $BaTiO_3$/polyacrylonitrile elastomer-based highly sensitive pressure sensor for intelligent sensing and posture recognition applications. *Nano Res.* **2023**, *16*, 5490–5502.